A model for intergalactic filaments and galaxy formation during the first gigayear

A. Gayler Harford[1]★ and Andrew J. S. Hamilton[1,2]★

[1]*JILA, University of Colorado, Boulder, CO 80309, USA*
[2]*Department Astrophysical and Planetary Sciences, University of Colorado, PO Box 440, Boulder, CO 80309, USA*

ABSTRACT

We propose a physically based, analytic model for intergalactic filaments during the first gigayear of the universe. The structure of a filament is based upon a gravitationally bound, isothermal cylinder of gas. The model successfully predicts for a cosmological simulation the total mass per unit length of a filament (dark matter plus gas) based solely upon the sound speed of the gas component, contrary to the expectation for collisionless dark matter aggregation. In the model, the gas, through its hydrodynamic properties, plays a key role in filament structure rather than being a passive passenger in a preformed dark matter potential. The dark matter of a galaxy follows the classic equation of collapse of a spherically symmetric overdensity in an expanding universe. In contrast, the gas usually collapses more slowly. The relative rates of collapse of these two components for individual galaxies can explain the varying baryon deficits of the galaxies under the assumption that matter moves along a single filament passing through the galaxy centre, rather than by spherical accretion. The difference in behaviour of the dark matter and gas can be simply and plausibly related to the model. The range of galaxies studied includes that of the so-called too big to fail galaxies, which are thought to be problematic for the standard Λ cold dark matter model of the universe. The isothermal-cylinder model suggests a simple explanation for why these galaxies are, unaccountably, missing from the night sky.

Key words: galaxies: dwarf – galaxies: formation – galaxies: haloes – galaxies: high-redshift – intergalactic medium – cosmology: theory.

1 INTRODUCTION

In the currently popular Λ cold dark matter (ΛCDM) model of the universe, collisionless dark matter dominates over baryons by a factor of nearly six (see Frieman, Turner & Huterer 2008 for review). A two-stage model for galaxy formation (White & Rees 1978) has survived as a general paradigm, in which the overall architecture of the universe is formed by the potential wells formed by the collisionless gravitation of the dark matter. For reviews, see Frenk & White (2012), Kravtsov & Borgani (2012), Conselice (2014), and Somerville & Davé (2015). The luminous structures that might be observed then would result from dissipational processes of the baryons trapped within these wells. This paradigm has justified the extensive use of *N*-body simulations using only dark matter to understand structure formation in the universe.

This paper challenges this paradigm in case of intergalactic filaments during the first gigayear. Using a cosmological simulation that includes gas hydrodynamics, radiative transfer, and chemistry in addition to dark matter, we show that the mass per unit length of intergalactic filaments depends upon the sound speed of the gas in the manner expected if the filaments were gravitationally bound, isothermal cylinders of gas (Stodólkiewicz 1963; Ostriker 1964) with dark matter mixed in.

An important implication of this model is that the filaments should have a preferred size as deduced from the simple analytic expression for their structure. This is because the mass per unit length of such a cylinder depends solely upon the temperature and ionization state of the gas, which in turn are constrained by the Lyman alpha cooling floor. A preferred size for intergalactic filaments is not expected from collisionless structure formation by dark matter alone.[1]

This study was motivated by our previous simulation studies (Harford, Hamilton & Gnedin 2008; Harford & Hamilton 2011),

★ E-mail: gayler_harford@post.harvard.edu (AGH); Andrew.Hamilton@Colorado.edu (AJSH)

---

[1] Dark matter does have a preferred length-scale arising from the sound horizon at recombination. However, this scale is vastly greater than that of galaxies and their attached filaments.
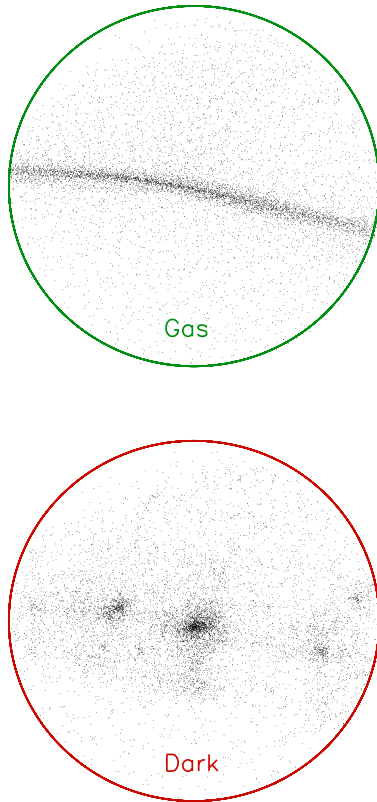
Figure 1. Visualization of structures of gas and dark matter. Shown are the gas and dark matter surrounding the centre of one of the larger galaxies in the simulation at redshift 5.134. Gas and dark matter are shown in separate images, each of which is a projection on to the page of a sphere having a comoving radius of 266 kpc centred on the centre of the galaxy. The normal to the page coincides with the normal to the principal plane of the gas.

studied, the gas is not heated because the smaller potential wells cannot sustain shocks (Birnboim & Dekel 2003). In this 'cold mode' scenario, gas passes directly into the galaxy without supersonic heating, perhaps mediated by intergalactic filaments (Birnboim & Dekel 2003; Binney 2004; Katz et al. 2003; Kereš et al. 2005; Dekel & Birnboim 2006; Ocvirk, Pichon & Teyssier 2008; Kereš et al. 2009; Dekel et al. 2009; Brooks et al. 2009).

A gravitationally bound, isothermal cylinder provides a physical framework for thinking about the motion of matter along an intergalactic filament. In this paper, we show that the gas is generally retarded in its entry into the galaxy centre relative to the dark matter. We suggest that it is the hydrodynamic pressure of the gas, counterbalancing the inward force of gravity that causes this behaviour.

We show that the different behaviours of dark matter and gas are consistent with a simple scheme for galaxy formation in which the dark matter collapses according to collisionless theory, while the gas tends to remain in extended, isothermal cylinders in which infall into the galaxy is retarded by the pressure of the gas.

In addition, we show that the different rates of accretion of dark matter and gas predict roughly the baryon deficits of the final galaxies under the assumption that matter moves along a single filament passing through the galaxy centre rather than by spherical accretion.

Understanding the structure of intergalactic filaments may not only provide insights into the mechanisms and pace of early galaxy formation, but may also place limits upon the sizes of galaxies that can form from a filamentary precursor. In this way, the model might be relevant to the so-called missing satellite problem (Kauffmann, White & Guiderdoni 1993; Klypin et al. 1999; Moore et al. 1999), which refers to the discrepancy between the observed number of satellite galaxies of the Milky Way and the predicted number of dark matter haloes from *N*-body simulations containing only dark matter. An additional, 'too big to fail' problem has also arisen in which a class of dark matter haloes thought to be massive enough to support star formation fail to be observed (Boylan-Kolchin et al. 2009). The model suggests a simple explanation for this anomaly. Resolution of these problems is critical to the viability of the cold dark matter hypothesis.

Most previous studies on intergalactic filaments have dealt with larger structures at later times in a more complex universe. Our study suggests that the intergalactic filaments associated with small galaxies during the first gigayear, and present during the critical period of reionization, may be a relatively simple model system to study.

The plan of the paper is as follows. In Section 2, we describe the self-consistent simulation of the first gigayear that we have analysed. Section 3 gives an overview of principal features of the model with illustrative diagrams. Section 4 compares the model to the simulation. Section 4.1 sets out exactly what we mean by a galaxy in the simulation and how we decide where it is at any given time.

Section 4.2 begins with a brief summary of the algorithm for identifying intergalactic filaments associated with specific galaxies. The algorithm is described in more detail with diagrams in Appendix A. Then the basic structural equations of a gravitationally bound, isothermal cylinder are laid out as developed by Stodólkiewicz (1963) and Ostriker (1964). The agreement of the filaments with such structures is then tested by comparing the total mass per unit length to that predicted by the model.

Section 4.3 shows that the collapse of the dark matter can be described by the textbook collapse of a spherically symmetric overdensity. Section 4.4 describes how we compare and contrast the collapse of gas and dark matter on to the final galaxy. Three categories of galaxies are distinguished in this regard: plunging gas,

which showed that gas and dark matter may assume very different structures shortly after the end of the first gigayear at a redshift of 5.134. For example, Fig. 1 shows separate images of gas and dark matter for the same projection of a sphere centred upon a galaxy. The gas appears as a relatively smooth filament, while the dark matter is more irregular, with discrete clumps positioned along the filament. We showed that the gravitational potential of the gas resembles that of a gravitationally bound, isothermal cylinder in cases where the filament is highly enriched in baryons.

In investigations that led to this paper, we began to explore the development of the filaments throughout the first gigayear of the simulation, in order to understand the origin of the isothermal structure. We found that baryon enrichment of filaments emerges late in the first gigayear. Earlier most of the filaments are not enriched, and yet, as we show in this paper, can be described as gravitationally bound, isothermal cylinders, provided that we make the simplifying assumption that the dark matter adds to the gravitational potential as if it were uniformly mixed with the gas.

Current thinking ascribes an important role to intergalactic filaments in the transport of gas into the small galaxies that form at high redshift. Two modes of gas entry into galaxies have been described in the literature. In the 'hot mode' incoming gas is shock heated when it encounters the potential well of the halo (Rees & Ostriker 1977). The shocked gas is elevated in temperature to where it can cool efficiently and then enter the halo. This mode is thought to predominate for galaxies larger than a few times 10^{11} M$_\odot$ and at low redshifts. It is thought that for smaller galaxies, like the ones we have

retreating gas, and lingering gas. Section 4.5 relates the findings to the baryon deficits of the final galaxies. The rates of movement of the gas and dark matter in the lingering-gas galaxies argue for collapse along a single filament as opposed to spherical accretion.

Section 4.6 relates the three categories of galaxies to the formation of isothermal cylinders and to the mass available to form filaments. Section 4.7 relates the model to the so-called too big to fail galaxies.

Section 4.8 explores an alternative model in which filament structure is determined primarily by dark matter.

Section 4.9 presents evidence that the filaments are aligned as predicted by the model.

Finally, the results are discussed and summarized in Sections 5 and 6, respectively.

2 COSMOLOGICAL SIMULATION

As in our previous work (Harford et al. 2008; Harford & Hamilton 2011), the results reported in this paper are based on a flat ΛCDM cosmological simulation that includes gas hydrodynamics, radiative transfer, and chemistry in addition to dark matter. The simulation followed an 8 h^{-1} comoving megaparsecs cube on a 256^3 grid up to a redshift of 5.13 using a 'softened Lagrangian hydrodynamics' (SLH-P^{3}M) code (Gnedin 1995; Gnedin & Bertschinger 1996). The cosmological parameters are $\Omega_m = 0.27$, $\Omega_b = 0.04$, $\sigma_8 = 0.91$, and $h = 0.71$.

Dark matter is computed with collisionless particles of mass $2.73 \times 10^6 \, M_\odot$. Gas dynamics is computed on a quasi-Lagrangian mesh that deforms adaptively to provide higher resolution in higher density regions. The mass of a gas particle is initially $4.75 \times 10^5 \, M_\odot$, but each gas particle mass may adjust slightly as the hydrodynamic computation evolves.

3 OVERVIEW OF MODEL

A simple paradigm for gravitational collapse begins with collapse in one dimension to produce a plane. Further collapse in a second dimension produces a rod, which then collapses in the third dimension to a quasi-spherical ball (Zel'dovich 1970; Park 1990; Bertschinger & Gelb 1991; Cen & Ostriker 1993). Visual inspection of the simulation suggested that this paradigm would be a good starting point.

It is common to assume that galaxies form at the intersections of filaments. This is because large-scale views of simulations at late times show galaxies as nodes in a complex network of filamentous material. This paper takes a different point of view for the first gigayear. We consider an individual filament to be an intermediate structure in the formation of a galaxy. In the model, an individual galaxy can be traced back in time to a single rod, in the centre of which a quasi-spherical galaxy will form as the contents of the rod collapse. After the first gigayear, multiple collisions may lead to the build-up of complex networks, which we will not consider here.

In the model, the rod is a gravitationally bound, isothermal cylinder of gas with comingled dark matter. Initially, the gas and dark matter are uniformly mixed. The dark matter then proceeds to collapse towards the centre of the rod, where the future galaxy will be found. The gas, in general, collapses more slowly than the dark matter because the pressure of the gas retards its flow into the galaxy.

The rod, in its initial form and during differential collapse, is shown schematically in Fig. 2. In the upper image the red, filled circles representing the dark matter are uniformly mixed with the green squares representing the gas. In the lower image, showing a
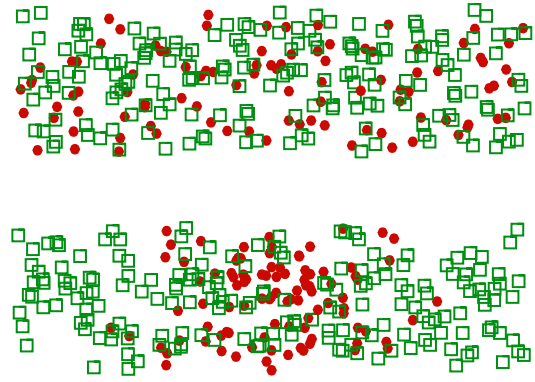

Figure 2. Schematic diagram of the model. These two images illustrate the model schematically in its purest form. The model is formulated as the collapse of a rod to form a quasi-spherical galaxy. Imagine that the centre of collapse is in the centre of each image. The upper image shows the rod at an early time with dark matter shown as red, filled circles and gas as green squares. The gas assumes the structure of a gravitationally bound, isothermal cylinder. The dark matter contributes gravitational effects but not hydrodynamic ones. To facilitate computation, we assume that the dark matter and gas are uniformly mixed, at least initially. The lower image shows the rod as it might appear at a later time. Dark matter has begun to collapse towards the centre, while the gas has remained extended because of the additional hydrodynamic effects that oppose the gravitational coalescence. In this paper, when the model is compared to the simulation, the two halves of the rod on either side of the centre of collapse are regarded as two separate filaments since both sides are not always present for every galaxy. The structure of such a filament is sampled at a position well separated from the centre of the forming galaxy. An example from the simulation that resembles this diagram is shown in Fig. 3.

later time, the dark matter particles have begun to coalesce into the centre of the rod leaving behind the gas particles. An actual example from the simulation is shown in Fig. 3.

4 COMPARISON OF THE MODEL TO THE SIMULATION

The purpose of this section is to compare the model proposed in Section 3 to the cosmological simulation described in Section 2.

4.1 Galaxies

The objects referred to as 'galaxies' in this paper were identified at the end of the simulation, at a redshift of 5.134 (1.15 Gyr after the big bang), from the total mass distribution by DENMAX (Bertschinger & Gelb 1991). The positions of the individual dark matter particles associated with each of these galaxies can be followed throughout the simulation. For a given galaxy defined by DENMAX at the end of the simulation, we define it at earlier times as the arrangement of its constituent dark matter particles at that time. The centre of the galaxy at any time is defined as the centre of mass of its dark matter particles, and the formation of each galaxy is followed with time in a local coordinate system relative to that centre of mass. In this coordinate system, the dark matter particles of each galaxy exhibit an initial expansion followed by a well-defined turnaround. The transient, quasi-spherical substructures seen at intermediate redshifts are not treated as separate galaxies.

In order to follow the development of single galaxies in time since the big bang, we focus on just the 1200 largest galaxies identified at the end of the simulation just after the first gigayear. The galaxies considered range in total mass from about $10^9 \, M_\odot$ to several times
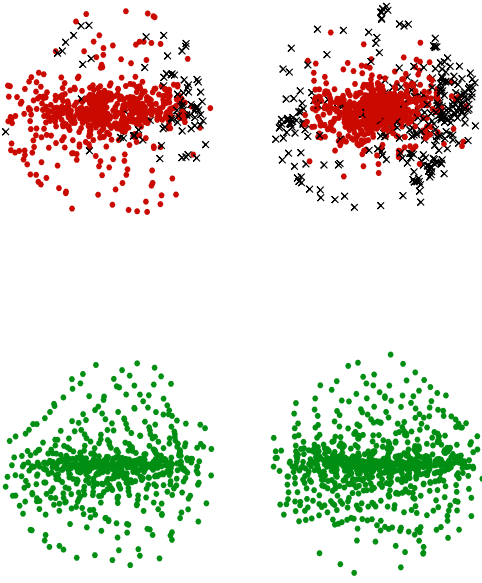
Figure 3. Images from the simulation that resemble the schematic drawing in Fig. 2. These are projections of a sphere centred on a single galaxy at an early time (left) and at a later time (right). The top two images show just the dark matter. The red, filled circles show particles that will actually end up in the galaxy at the end of the simulation. They are seen to coalesce in the centre at a later time in the image on the right. The black X's are other dark matter particles. Some of these may contribute gravitationally to the structure of the filament. The bottom two images show just the gas particles as green, filled circles. They assume a relatively smooth filamentary structure throughout.

10^{11} M$_\odot$. The total mass of the galaxy is defined to include dark matter, gas, and stellar material.

4.2 Isothermal filaments

To avoid subjective bias in identifying filaments, we adopt an objective algorithm which is detailed in Appendix A. Shortly after turnaround of the dark matter, the single rod of the model appears embedded in a planar slab of material. We take advantage of this situation to select the filaments in the two dimensions of the principal plane. The filaments are selected using only the gas component because its structure is more regular than that of the dark matter. Although the model in its purest form is best understood as the collapse of a single rod, we will refer to the two halves of the rod as separate filaments because both halves are not always present in the structures surviving our selection algorithm. No more than two filaments are selected for a single galaxy. When two are present, the filaments are usually oriented end-to-end as if part of a single, continuous structure.

The mass per unit length, Υ, predicted for a gravitationally bound, isothermal gas cylinder is

$$\Upsilon = \frac{2c_s^2}{G} \qquad (1)$$

where c_s is the isothermal sound speed and G is the gravitational constant (Stodólkiewicz 1963; Ostriker 1964). The sound speed c_s at temperature T is

$$c_s = \sqrt{\frac{kT}{1.22 \mu m_H}} \qquad (2)$$

where k is the Boltzmann constant, m_H the mass of the hydrogen atom, and μ a mean particle mass to take into account the ionization

of the hydrogen. The factor of 1.22 corrects for the contribution of neutral helium to the mean atomic weight.

The important point here is that the mass per unit length of a filament depends only upon its temperature and ionization state, and not upon the concentration of the gas in the transverse direction.

The presence of dark matter adds gravitational field without any additional pressure. The simplest way, and the way we adopt, to account for the effect of dark matter is to assume that the gas and dark matter are uniformly mixed. The result of this assumption is that equation (1) predicts, not the mass per unit length of the gas, but the total mass per unit length including the dark matter.[2] It is interesting to note that this scheme means that if the relative amounts of gas and dark matter in the filament vary, then they must vary in opposite directions to keep the total in line with the sound speed. This situation contrasts with the conventional assumption that gas follows dark matter.

Appendix A describes the algorithm for selecting regions of the filaments to study. For detailed analysis, a filament segment is defined as the gas and dark matter within a cylinder of length 12 proper kiloparsecs and a radius of 6 proper kiloparsecs centred on the filament region selected as described in Appendix A. Even though the mass of the cylinder extends to infinity in theory, we find that most of the mass is within this proper radius. The orientation of the axis of the cylinder is determined by a principal component analysis.

We might expect the development of a filament to depend upon the local thermal history. Reionization occurs during the first gigayear. However, different regions of the simulation reionize at different times. For this reason, we present the structure of the filaments using the square of the sound speed as a proxy for time. This scheme accommodates the possibility that different filaments are at different stages of development at the same time. The sound speed depends only upon the temperature and ionization state of the gas and is independent of the density. It is computed as the average of the squares of the sound speeds of the individual gas particles in the filament segment being analysed. The sound speed of a gas particle is computed from its temperature and ionization state, which are independently computed. In the simulation, the temperature and ionization are computed self-consistently from the radiation produced at specific loci of star formation. There is no superimposed, ionizing field as in many other simulations.

The course of reionization of the individual filament segments is shown in the scatter plot in Fig. 4, in which each point is a filament segment at one of the six redshifts we studied. The abscissa is the average of the square of the sound speeds of the gas particles in the segment. The ordinate shows the mean mass per particle (nuclei and electrons) in the gas of the segment, which decreases as a result of reionization. It is clear that the segments at any given redshift are present in a range of different stages of reionization. In this paper, the square of the sound speed is always expressed in the same units chosen to facilitate comparisons with the predictions of the model in Figs 5 and 7.

Fig. 5 is at the crux of the argument for gravitationally bound, isothermal cylinders. It shows, over a range of sound speeds, that the total mass per unit length of the filament segments can be predicted from the sound speed of the gas using equation (1). The value computed for the gas from this equation is divided by the overall gas fraction of the segment to give the total mass per unit length plotted in the figure. The units of the axes have been chosen for

---

[2] The amount of stellar material in the filaments in negligible, and we neglect it.
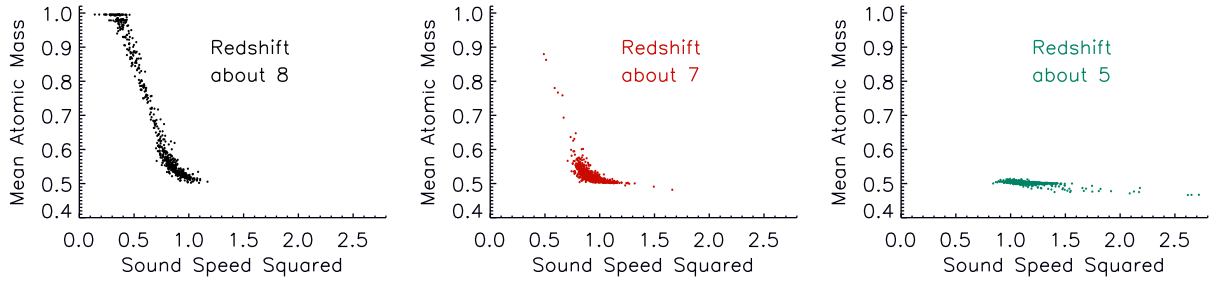
Figure 4. History of reionization. Scatter plots showing the course of reionization as a function of the sound speed squared for three redshift ranges. Each dot represents an individual filament segment. The abscissa values represent the sound speed squared using the arbitrary units of Fig. 5. The ordinate values are mean atomic mass (μ in equation 2). The left-hand panel pools the data at redshifts 8.90 and 8.09, the middle panel at 7.33 and 6.69, and the right-hand panel at 5.85 and 5.13.
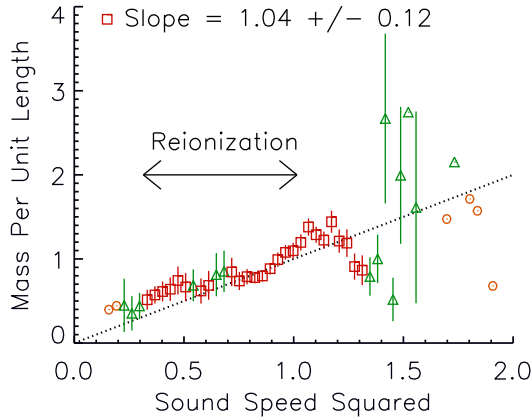

Figure 5. Proportionality of total mass per unit length to square of sound speed. The symbols show the average total (gas plus dark matter) mass per unit length for the filaments in each bin of sound speed squared. The units have been chosen to illustrate the expectation of proportionality for the model, shown as the diagonal, dotted line with a slope of one. A value of one on the abscissa corresponds to a sound speed of 12.9 km s^{-1}. A value of one on the ordinate corresponds to 7.71×10^7 M$_\odot$ kpc^{-1} in proper units. The bin size is 0.035. The vertical line through each symbol represents one standard error for the average of the filaments in that bin. Standard errors are computed for each bin having more than two members. Each red square represents a bin containing at least 15 filaments. The green triangles represent other bins having at least two filaments, for which a standard deviation can be calculated. The remaining orange, open circles represent bins with a single filament. The bins with at least 15 filaments apiece have a linear regression line constrained to pass through the origin with a slope of 1.04 ± 0.11 with a *P*-value of 1.7×10^{-19} and RSquared of 0.96. The probability that the residuals belong to a normal distribution is 0.21. Regression analysis was performed using MATHEMATICA (Wolfram Research).

convenience so that the model predicts a slope of one. The ordinate shows the average for filaments segments in bins of sound speed squared on the abscissa. Bins having at least 15 members, shown by red squares, were chosen for a linear regression analysis. The slope obtained, 1.04 ± 0.12, shows good agreement with prediction.

The prediction, shown by the dotted, diagonal line of unit slope in Fig. 5 assumes for simplicity that the dark matter is uniformly intermixed with the gas and contributes to the gravitational field in proportion to its abundance.[3] An alternative scheme, in which the gas is concentrated in a relatively flat central part of a dark

[3] It is impractical to subdivide the filament segments into regions with different amounts of dark matter even though the dark matter is clumpy. The gas tends to be smoother and not to clump with the dark matter.
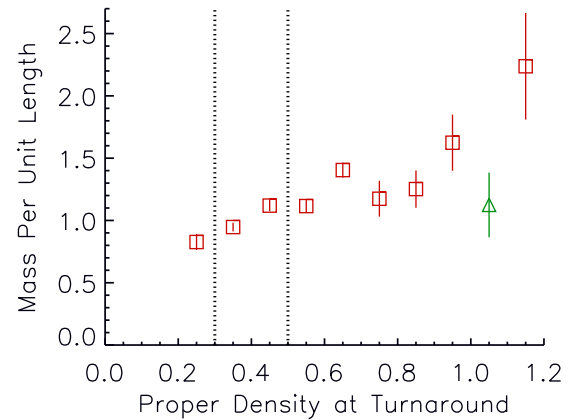
Figure 6. Total mass per unit length as a function of proper density at turnaround. Proper density at turnaround on the abscissa is in units of 10^6 M$_\odot$ kpc^{-3}. Total mass per unit proper length of the filament segment on the ordinate is in the same units as for Fig. 5 and the symbols are as described for that figure. Single standard errors are shown by vertical lines. The vertical, dotted lines indicate the range of turnaround densities used to create Fig. 7.

matter potential well would predict for most segments a gas mass per unit length greater than observed by a factor of about five since, in the latter scheme, the gas behaves as if it were a pure gas cylinder without dark matter. The measured mass per unit length is more consistent with the model where the gas and dark matter are uniformly mixed.

In Fig. 5, the sparser bins to the right (green triangles) show only a general upward trend consistent with prediction. Orange circles indicate bins with a single member.

The period of best agreement with the model corresponds to the period of active reionization when the gas in the segments is partially ionized. The extent of this region is indicated by the horizontal, two-headed arrow. During this period, most of the change in sound speed is due to reionization. The temperature changes little.

One should not conclude from these results that the model applies only to the reionization period. During the limited period of the simulation only a few of the filaments have progressed significantly beyond reionization, and these are associated with the largest galaxies. We will argue in Section 4.6 that excessive mass can lead to deviation from the model. However, the small numbers of segments in these sparse bins make it difficult to tell just how well the model works for the largest galaxies.

Another variable that might be expected to affect the filament structure is the proper density at turnaround. Fig. 6 shows that
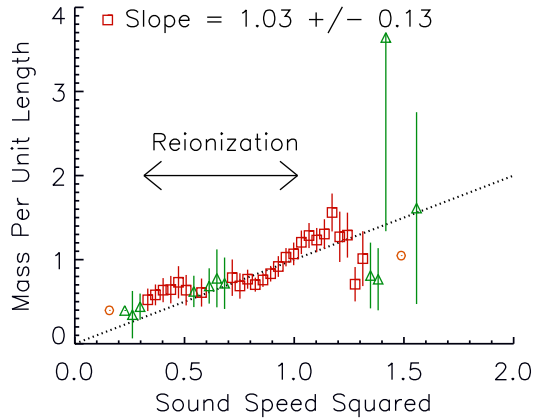
Figure 7. Proportionality of total mass per unit length to square of sound speed when controlled for density at turnaround. This figure is the same as Fig. 5 except that the filaments have been drawn from a restricted range of proper density at turnaround, namely 3.0–$5.0 \times 10^5 \, \mathrm{M_{\odot} \, kpc^{-3}}$. The symbols show the average total (gas plus dark matter) mass per unit length for the filament segments in each bin of sound speed squared. The units are the same as described for Fig. 5. The vertical line through each symbol represents one standard error for the average of the filaments in that bin. Standard errors are computed for each bin having more than two members. Each red square represents a bin containing at least 15 segments. The green triangles represent other bins having at least two segments, for which a standard deviation can be calculated. The remaining orange, open circles represent bins with a single segment. The bins with at least 15 segments apiece have a linear regression line constrained to pass through the origin with a slope of 1.03 ± 0.13 with a P-value of 7.1×10^{-18} and RSquared of 0.96. The probability that the residuals belong to a normal distribution is 0.23. The regression line is constrained to pass through the origin.

the total mass per unit length does indeed increase with density at turnaround as one might expect. To demonstrate that the correlation of Fig. 5 is not an artefact resulting from a correlation of sound speed with density at turnaround, we tested filaments from a restricted range of turnaround densities. Fig. 7 shows a version of Fig. 5 in which only galaxies within a narrow range of turnaround densities, those between the two vertical, dotted lines in Fig. 6, are included. Figs 5 and 7 are almost identical.

4.3 Collapse of dark matter

The simplest theory of galaxy formation in an expanding universe is that of the collapse of a spherically symmetric overdensity (Peacock 1999). Sugerman, Summers & Kamionkowski (2000) find that, despite its simplifying assumptions, the spherical model provides reasonable predictions for properties of dark matter haloes. The spherical model predicts that the radius r of a mass m evolves with time t as a cycloid (Peacock 1999),

$$r = \frac{r_{\mathrm{turn}}}{2}(1 - \cos\theta), \quad t = \sqrt{\frac{r_{\mathrm{turn}}^3}{8Gm}}(\theta - \sin\theta). \quad (3)$$

The cycloid describes expansion from zero to a maximum radius, the turnaround radius r_{turn}, as θ goes from 0 to π, followed by contraction as θ goes from π to 2π. To compare this theory with a given galaxy in the simulation, the average radius of the dark matter particles is computed at a series of times before and after turnaround. To compare these radii to the cycloid prediction, the mass m in equation (3) is computed from the actual turnaround sphere using the theoretically expected overdensity of 5.55 (Peacock 1999).
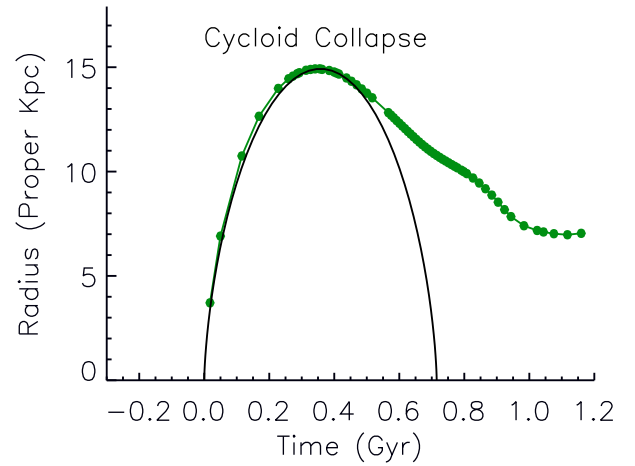

Figure 8. Spherical collapse of dark matter in an example galaxy. The average proper radius of galaxy dark matter particles as a function of time after the big bang is plotted as a green solid line with green filled circles. The corresponding cycloid is shown by the solid black line.

We find the spherical model to be an excellent starting point for understanding the collapse of the dark matter of each galaxy. Fig. 8 shows, for an example galaxy, the average radius of the galaxy's dark matter particles from their centre of gravity and the corresponding cycloid. Virtually all the galaxies fit a cycloid at least up until turnaround.

The fitted cycloid is translated slightly in time so that the turnaround time coincides with that in the simulation. We find that the cycloid generally begins its ascent either at the beginning of the simulation or slightly before. We interpret this result to mean that the galaxies originate from fluctuations imposed at the start of the simulation, rather than from density variations resulting from subsequent events.

Fig. 9 shows histograms of the overdensity, time, and radius at turnaround. The approximate agreement of the overdensity with the theoretical value of 5.55 (Peacock 1999) supports our interpretation for the dark matter collapse as the collapse of a spherically symmetric overdensity.

4.4 Contrasting motion of dark matter and gas

Unlike the dark matter particles, the individual gas particles in the simulation cannot be traced throughout the simulation. Rather, they are generated anew after each hydrodynamic time-step. Since the structures are continually moving and changing shape, it is difficult to pin down gas movements on a small scale. What we can compute unambiguously, however, is an overall measure of collapse. We compute this separately for the gas and the dark matter so that we can compare their relative rates of motion into the centre of the galaxy.

At each redshift, we compute as a function of redshift the proper radius of a sphere centred on the galaxy that includes just that mass of gas or dark matter that was present inside the turnaround radius at the time of turnaround (the turnaround radius is the average radius of the dark matter particles of a galaxy at the time of turnaround).

Fig. 10 shows some individual galaxy histories that illustrate the types of results obtained. The abscissa shows the cosmic scale factor starting from the time of turnaround, which is slightly different for different galaxies. The ordinate is the radius as a fraction of
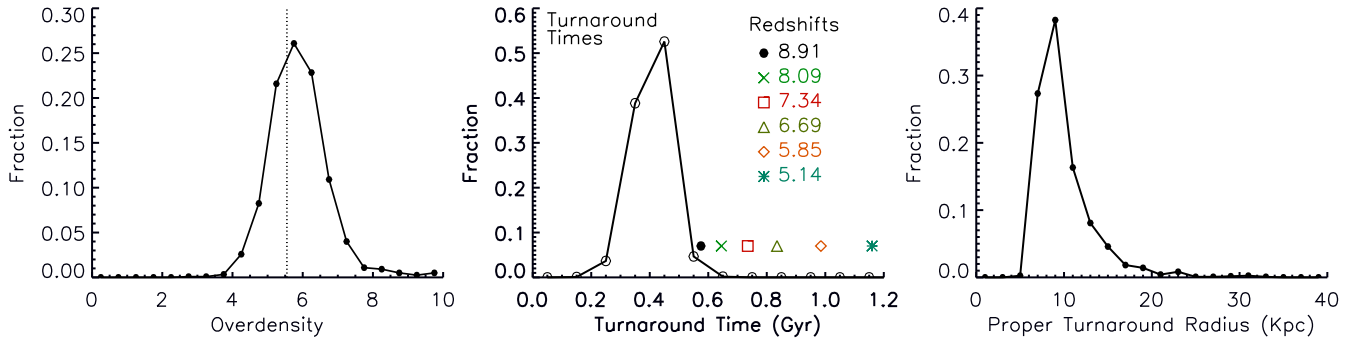
Figure 9. Histograms of (left) overdensity, (middle) time, and (right) radius at turnaround for the 1200 largest galaxies in the simulation. In the left-hand panel, the overdensity is computed for a spherical volume centred at the centre of mass of the dark matter particles and having a radius equal to the average radius of the dark matter particles of the galaxy. The theoretically predicted overdensity of 5.55 (Peacock 1999) is shown by the vertical dotted line. In the middle graph, the times corresponding to the six redshifts at which structural analysis of filaments was done are shown for comparison to the histogram of turnaround times.
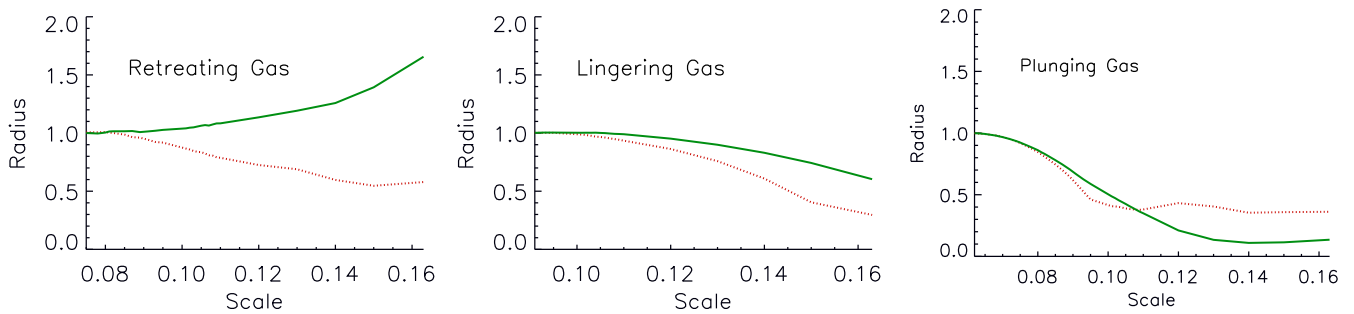

Figure 10. Overall collapse of dark matter and gas in three categories of galaxy. Each graph describes a single galaxy chosen to illustrate a category. Shown is the contrasting motion of dark matter (dotted, red lines) and gas (solid green lines) towards the centre of the galaxy. At a series of redshifts starting at turnaround the lines show the progression of the radius of just that mass of gas or dark matter that was within the turnaround radius. The units of the radius are fractions of the turnaround radius. All radii are proper. The abscissa shows the redshifts as cosmic scale factors. The significance of these categories will be discussed in Sections 4.6 and 4.7.

the turnaround radius. Most of the time, the gas collapses more slowly than the dark matter as shown in the first two graphs. In the left graph, the gas does not collapse fast enough to outrun the expansion of the universe, and the gas radius increases with time. We call this the 'retreating-gas' type of galaxy. We will see that these are among the least massive of the galaxies we have studied. In the 'lingering-gas' type, shown in the middle graph, the gas collapses but more slowly than the dark matter. We will see in later sections that the filaments associated with these galaxies have the best fit to an isothermal cylinder. Finally, the right graph shows the gas collapsing more rapidly than the dark matter, the 'plunging-gas' case. There are 416 retreating-gas galaxies, 722 lingering-gas galaxies, and 62 plunging-gas galaxies.

We will refer to the sphere containing the turnaround amount of mass as the *collapse sphere* for the gas or dark matter as the case may be for the time in question. The proper radius of the collapse sphere divided by the proper turnaround radius we will call the *collapse fraction*. When the radius is taken at the end of the simulation, we will refer to this ratio as the *final collapse fraction* of the gas or dark matter.

Fig. 11 shows histograms of the final collapse fractions of dark matter and gas for the 1200 galaxies studied in this paper. The histogram for the dark matter (the red curve with squares) peaks at a collapse fraction of about one half, in agreement with the virial expectation for collisionless particles subject only to gravitation. In contrast, the gas (green curve with triangles) generally collapses more slowly.
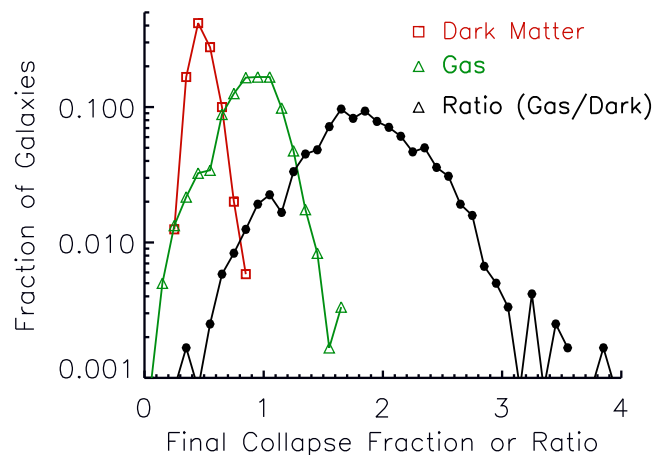

Figure 11. Comparison of the movement of dark matter and gas into the galaxy. Histograms show the final collapse fractions of dark matter (red squares) and gas (green triangles), and the ratio of the two for individual galaxies (black, filled circles). The graphs show that for 94.6 per cent of the galaxies, the dark matter collapses more rapidly than the gas. The final collapse fraction is defined in Section 4.4.

The black curve with filled circles in Fig. 11 shows a histogram of the ratio of the collapse fraction of the gas to that of the dark matter for the same galaxy. The small fraction of the area under the curve to the left of a ratio of 1.0 shows that most of the time the
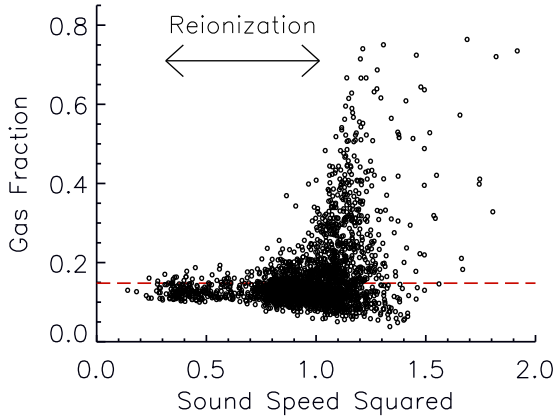
Figure 12. Gas fraction as function of sound speed. Each black, circle represents an individual filament segment. The abscissa is the square of the sound speed and the ordinate is the gas fraction. The arrow shows the extent of the period of reionization of the filament segments. The cosmic baryon fraction is indicated by the red, dashed line. There is little stellar material in the filaments at these times, and its presence has been ignored.
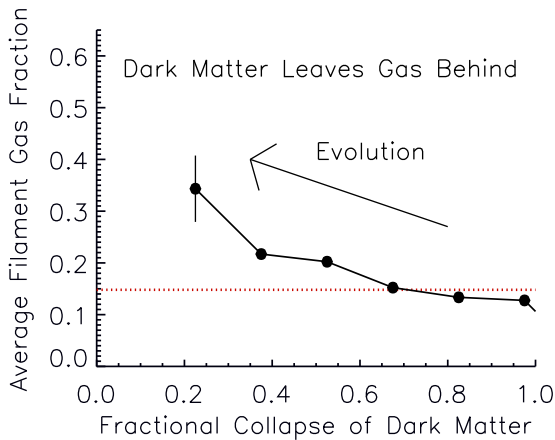

Figure 13. Dark matter leaves gas behind to produce baryon enrichment of filaments. The graph shows the average gas fraction of filament segments as a function of the collapse fraction of the dark matter of the galaxy at the redshift of the segment. Collapse fraction is defined and determined as specified in Section 4.4. Note that in this figure, maximal collapse is at the left and minimal collapse at the right. The horizontal, dotted, red line indicates the cosmic baryon fraction.

gas collapses more slowly than does the dark matter. We suggest that the pressure in the gas filament counterbalancing the force of gravity is responsible for this difference in behaviour.

The end of reionization marks the beginning of a period of increasing deviation of the gas fraction of the filament from the cosmic value as shown in the scatter plot in Fig. 12. Here, each open circle represents a filament segment.

We suggest that this effect occurs when rapidly collapsing dark matter effectively leaves behind the gas in the filaments. Fig. 13 shows the average gas fraction of filament segments as a function of the collapse fraction of the dark matter of the associated galaxy at the redshift of the filament. As the dark matter of a galaxy collapses, the filaments of that galaxy can become more baryon rich. Note that in this figure maximal collapse is at the left and minimal collapse at the right.
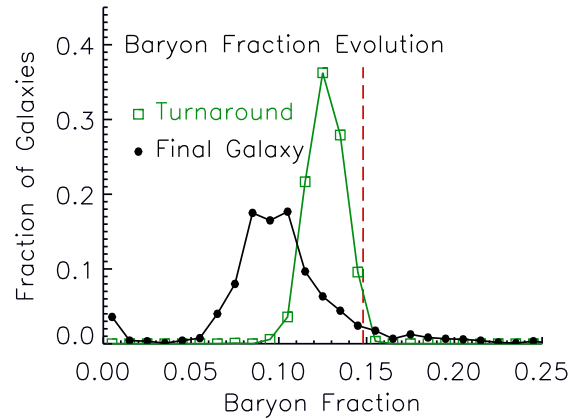

Figure 14. Baryon fraction at turnaround and in final galaxy. Histograms compare the baryon fraction at turnaround with that of the final galaxy for all of the galaxies in this study. The green line with squares represents the baryon fraction of the matter within the turnaround radius. The black line with filled circles represents the baryon fraction of the final galaxies at the end of the simulation as determined by the galaxy finding algorithm. The vertical, red, dashed line indicates the cosmic baryon fraction.

4.5 Filamentary as opposed to spherical accretion

Unlike many of the final galaxies, the turnaround sphere has a baryon fraction close to the cosmic value. The differential collapse of gas and dark matter can lead to significant baryon deficits in the final galaxies. Fig. 14 compares histograms of the baryon fraction at turnaround and in the final galaxies.

The differing motions of the dark matter and gas that we have just described in Section 4.4 can be related in a simple way to these baryon deficits. Consider, for simplicity, the lingering-gas situation in which the dark matter collapses faster than the gas. At the end of the simulation, the final collapse sphere for the galaxy's dark matter will have a baryon fraction less than that of the turnaround sphere and closer to that of the baryon fraction of the final galaxy. The gas in this sphere is some fraction of the gas at turnaround. If, for simplicity, we assume that the gas in both the initial turnaround sphere and the final dark matter collapse sphere is in the form of a uniform filament that runs along the diameter of both spheres, then the fraction of the turnaround gas that is in the dark matter collapse sphere can be estimated from the ratio of the radius of this sphere to that of the larger gas collapse sphere. Thus, the baryon fraction of the final dark matter collapse sphere, can then be computed knowing the baryon fraction at turnaround.

Fig. 15 shows that this simple filamentary scheme predicts the baryon fraction of the final dark matter collapse sphere quite well. Each point on the graph represents a single galaxy. The abscissa is the predicted baryon fraction and the ordinate is the actual one. The red, dashed line represents agreement between the two. Excluded from this plot are plunging-gas galaxies where the gas collapses as fast as or faster than the dark matter. These are mostly the largest galaxies. Also excluded are the retreating-gas galaxies where the gas fails to turn around even though the dark matter does. These are the galaxies where the final collapse fraction of the gas is greater than or equal to one.

Fig. 16 shows the contrasting predictions if the relevant ratio of radii were instead cubed, as would be more appropriate for spherical accretion. The filamentary accretion model is a much better fit than is the spherical one.

The baryon fractions shown in Figs 15 and 16 are for the final dark matter collapse sphere and are somewhat lower than those of the
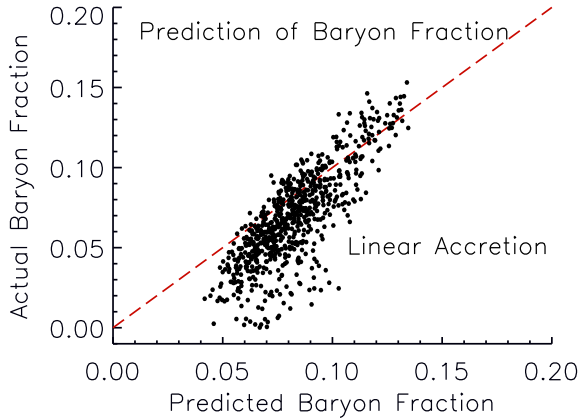
Figure 15. Predicting baryon fraction assuming filament accretion. As described in Section 4.4, the baryon fraction of the final collapse sphere for the dark matter is predicted from the baryon fraction at turnaround and the final collapse fractions of the dark matter and gas. The computation assumes movement of the gas along a uniform filament. Each point represents a single galaxy. The abscissa shows the predicted value and the ordinate the actual one. The dashed, red line represents agreement of the prediction with the actual. The 5.4 per cent of galaxies for which the dark matter does not collapse faster than the gas are excluded as well as the galaxies where the gas, unlike the dark matter, does not turn around at all.
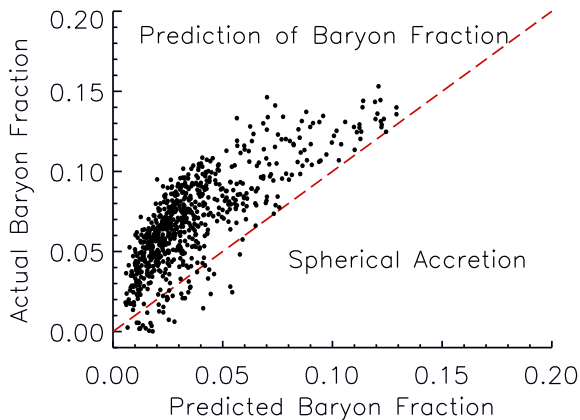

Figure 16. Predicting baryon fraction assuming spherical accretion. As described in Section 4.4, the baryon fraction of the final collapse sphere for the dark matter is predicted from the baryon fraction at turnaround and the final collapse fractions of the dark matter and gas. The computation assumes spherical accretion of the gas on to the galaxy. Each point represents a single galaxy. The abscissa shows the predicted value and the ordinate the actual one. The dashed, red line represents agreement of the prediction with the actual. The 5.4 per cent of galaxies for which the dark matter does not collapse faster than the gas are excluded, as well as the galaxies where the gas, unlike the dark matter, does not turn around at all.

final galaxies as identified by the galaxy finding algorithm DENMAX. Since the turnaround sphere is based upon the average radius of the dark matter particles at turnaround, we might expect the final dark matter collapse sphere to represent an inner sphere of the galaxy. DENMAX might be adding to this a more baryon-rich region at the periphery of the galaxy.

From the results of this section, we suggest that a major cause of baryon deficits in the galaxies we have studied is the retarded motion of the gas relative to the dark matter. This situation is in contrast to a mechanism whereby gas already in the halo is subsequently expelled.
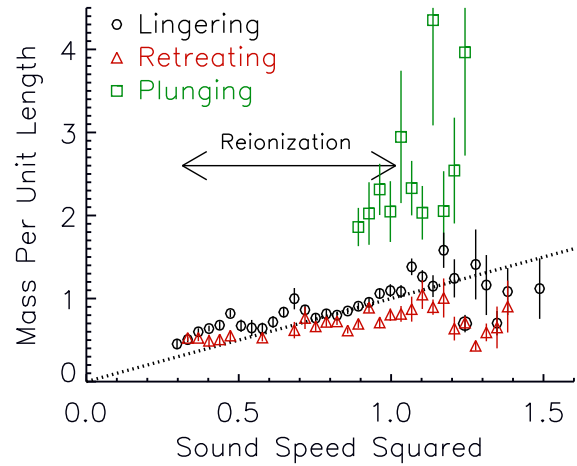
Figure 17. Total mass per unit length as a function of sound speed. The symbols show the average total mass (dark matter plus gas) for filaments associated with galaxies of the three types: black open circles for lingering gas, green squares for plunging gas, and red triangles for retreating gas. As for Figs 5 and 7, the units on the axes have been chosen to illustrate the expectation of proportionality for the model, shown as the diagonal, dotted line. Only bins having at least five members are shown for each type. Vertical bars are single standard errors. The range of sound speeds during the process of reionization is indicated by the black arrow.

4.6 Isothermal cylinders retard gas

In Section 4.4, we distinguished three types of galaxies. The ones where the gas moves towards the galaxy as fast or faster than the dark matter we referred to as 'plunging-gas' galaxies. Those where the gas shows no net movement towards the galaxy we referred to as 'retreating-gas' galaxies. Those where the gas moves towards the galaxy but not as fast as the dark matter we referred to as 'lingering-gas' galaxies.

The filaments of these three galaxy types have been tested separately for evidence of gravitationally bound, isothermal cylinders. Fig. 17 shows the correlation of the mass per unit length with the square of the sound speed. The filaments from the lingering-gas galaxies (black, open circles) show the best match. The filaments of the retreating-gas galaxies (red triangles) fail to keep up with the expansion of the universe. The plunging-gas galaxies, shown by the green squares have too much mass for isothermal cylinders.

These contrasting results can be understood in terms of the key property of a gravitationally bound, isothermal cylinder that the mass per unit length is limited by the sound speed of the gas. We might expect the cylinder to break down if the overall collapsing mass is overwhelmingly larger than can be accommodated at the current sound speed. This situation would correspond to the plunging-gas case. On the other hand, the filaments of the retreating-gas galaxies might have too little matter to withstand the expansion of the universe.

If an isothermal cylinder does form, one would expect the hydrodynamic forces that stabilize it to compete with the gravitational pull of the dark matter that is collapsing to form the halo of the galaxy. This effect would be expected to retard the flow of the gas relative to that of the dark matter. Only the excess gas that cannot be accommodated into the cylinder structure would be free to proceed unhindered. This situation might describe the filaments of the lingering-gas galaxies.

A measure of the mass per unit length available to form a filament can be obtained by dividing the total mass of the turnaround sphere
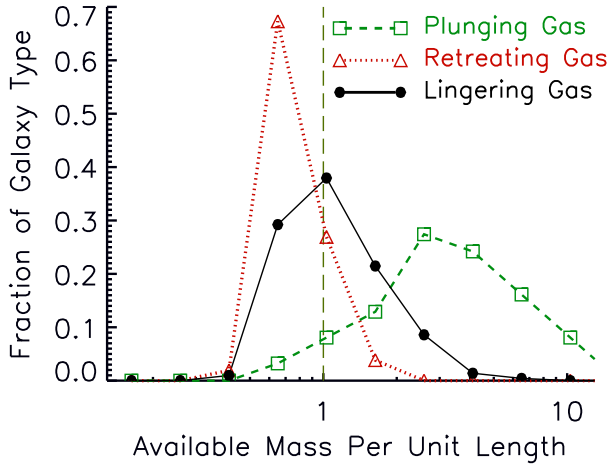
Figure 18. Available mass per unit length for the three galaxy types. Histograms of the available mass per unit length for the three galaxy types. The abscissa is the available mass per unit length in the units used in Figs 5, 7, and 17 to compare the mass per unit length to the sound speed. The ordinate is the fraction of that galaxy type. The black, solid line with filled circles represents lingering-gas galaxies. The green, dashed line with squares represents plunging-gas galaxies. The red, dotted line with triangles represents the retreating-gas galaxies. The vertical, dark green, dashed line at 1.0 is the mass per unit length corresponding to one unit in the figures showing the correlation with the square of the sound speed.
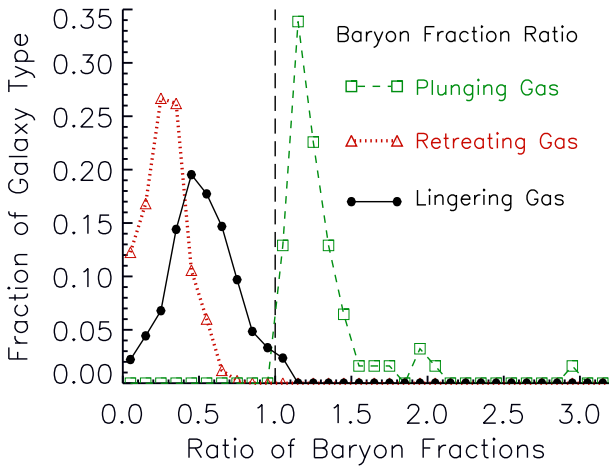

Figure 19. Change in baryon fraction after turnaround. The abscissa of these histograms show the ratio of the baryon fraction of the final collapse sphere to that of the turnaround sphere. The ordinate shows the fraction of galaxies of each of the three types. The vertical, black, dashed line indicates no change during this period.

by its proper diameter, a quantity we will call the *available mass per unit length*. Fig. 18 shows histograms of the available mass per unit length for the three galaxy types. The histogram for the lingering-gas galaxies peaks at the mass per unit length value corresponding to a sound speed squared of one in Figs 5, 7, and 17. This value, which marks the end of reionization, is indicated by the vertical, dark green, dashed line. The retreating-gas galaxies peak to the left and the plunging-gas galaxies to the right.

The change in baryon fraction between turnaround and the final collapse sphere for the three galaxy types is shown in Fig. 19. As expected, the retreating-gas galaxies lose the most baryons and the lingering-gas galaxies lose fewer baryons. The plunging-gas galaxies actually gain baryons.
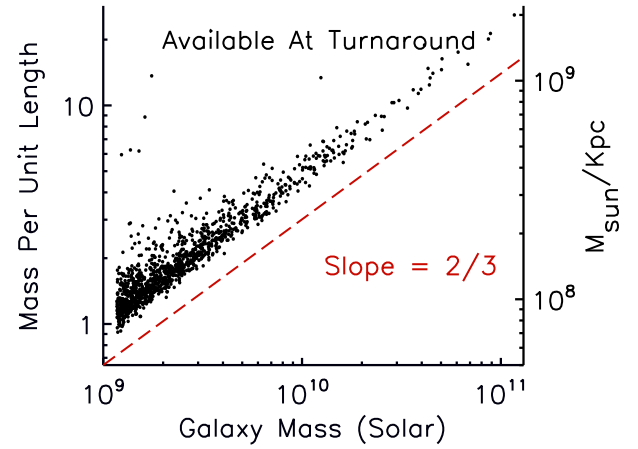

Figure 20. Available mass per unit length at turnaround as a function of the total mass of the galaxy. Each symbol represents a single galaxy. The available mass per unit length is considered to be the ratio of the total mass within the turnaround radius to the diameter of the turnaround sphere. The left ordinate shows mass per unit length in the units used in Figs 5, 7, and 17 to compare the mass per unit length to the sound speed. The right ordinate shows the mass per unit length in units of solar per kiloparsecs for comparison. If the collapse is self-similar, the expected slope of this log–log plot is two-thirds.

As expected, available mass per unit length increases with the total mass of the final galaxy. This relation is shown in Fig. 20. Since the turnaround radius, and hence the mass within it as well, is determined by the average radius of the galaxy's dark matter at turnaround, a simple hypothesis is that the log of the available mass per length should be proportional to the log of the total galaxy mass with a slope of two-thirds. The figure, in which each symbol represents a single galaxy, shows approximate agreement with this simple, self-similar picture.

4.7 Too big to fail galaxies

Considerable success has been seen in attempts to match observed galaxies to haloes seen in simulations based upon the ΛCDM model (for a review see Somerville & Davé 2015). A circular velocity for observed galaxies can be derived from the Doppler broadening of H I lines. A reasonable relation between this measurement and the circular velocity of simulated haloes can be adduced which leads to rough agreement between the number densities of observed and simulated galaxies as a function of circular velocity.

However, important discrepancies remain at low halo masses. The term 'too big to fail' has been applied to haloes having a circular velocity between about 25 and 45 km s^{-1} (Boylan-Kolchin et al. 2009; Boylan-Kolchin, Bullock & Kaplinghat 2011, 2012; Ferrero et al. 2012; Garrison-Kimmel et al. 2014; Tollerud, Boylan-Kolchin & Bullock 2014; Papastergis et al. 2015; Klypin et al. 2015; Papastergis & Shankar 2016). The frequency of these galaxies in observations is much lower than what would be predicted from the ΛCDM model. The choice of terminology comes from the paradox that these galaxies are not seen despite apparently being massive enough to retain much or all of their gas throughout reionization. This situation is in contrast to galaxies with lower circular velocities, whose relative absence from observation is more easily explained by reionization.

The 'too big to fail' concept is based on observations of present-day galaxies, whose detailed histories are uncertain. However, the
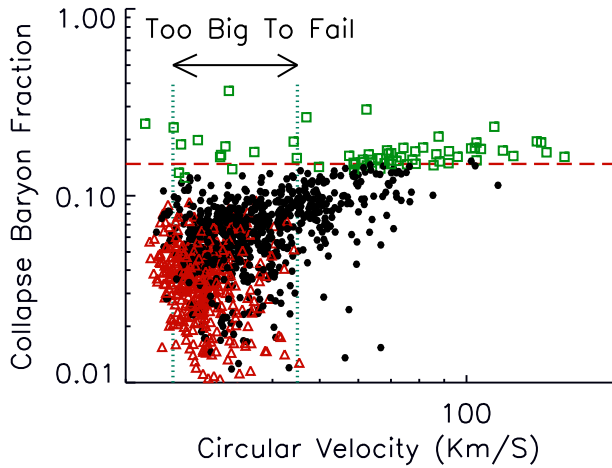
Figure 21. Scatter plot of the final baryon fraction of galaxies as a function of the halo circular velocity. The 'too big to fail' galaxies are considered to be those with circular velocity between 25 and 45 km s^{-1} (Papastergis & Shankar 2016) as indicated by the blue, dotted, vertical lines. Shown on the ordinate is the baryon fraction of the final dark matter collapse sphere (see Section 4.4 for definition). The red, dashed line indicates the cosmic baryon fraction. The circular velocity on the abscissa is computed from the dark matter in this sphere using equation (4). The green squares represent the plunging-gas galaxies, namely those where the gas collapses as fast or faster than the dark matter. The red triangles represent the retreating-gas galaxies, namely those where the gas fails to turn around unlike the dark matter. The black, filled circles are the galaxies between these two extremes, which we have called lingering-gas galaxies. These are the ones we suggest are the 'too big to fail' galaxies and which show the best agreement with an isothermal cylinder. They are also the ones used to produce Figs 15 and 16, which show that the baryon fraction can be predicted from the assumption that the matter collapse occurs along a filament rather than spherically. The reduction of the baryon fraction below the cosmic value for these galaxies might make them invisible. Note that the left end of the abscissa begins at 20.

simulated galaxies we studied are expected to include the mass range of the 'too big to fail' phenomenon, and so might be relevant models. The scatter plot of Fig. 21 shows the baryon fraction of the final collapse sphere as a function of the circular velocity of its dark matter as estimated from equation (4).

$$V_c = \sqrt{\frac{G M_d}{R}} \qquad (4)$$

where V_c is the circular velocity, M_d the mass of dark matter, R the radius of the sphere, and G the gravitational constant. The approximate circular velocity range of the 'too big to fail' galaxies is delimited by the vertical, light blue, dotted lines. These galaxies have significant baryon deficits that might make them difficult to observe. The green squares represent the galaxies where the gas collapses as fast or faster than the dark matter, i.e. the plunging-gas galaxies. The baryon fraction for these galaxies is close to the cosmic value. The red triangles represent the retreating-gas galaxies, where the gas fails to turnaround. As might be expected, these are clustered at the low end of the circular velocity range and have the greatest baryon deficits. The black, filled circles are the lingering-gas galaxies. We suggest that the lingering-gas galaxies are the 'too big to fail' galaxies.

We suppose that the formation of gravitationally bound, isothermal cylinders inhibits the collapse of gas into haloes otherwise thought to be massive enough to have plenty of gas. These galaxies are then missing from observations because they form too few stars,

that is, they are 'too big to fail' but fail because of the structure of the filaments.

4.8 An alternative dark matter model

In this section, we consider an alternative filament model in which the gas is passively trapped in an overwhelming dark matter potential determined by the aggregation properties of dark matter. Could such a model be consistent with the filaments we have studied?

We do not favour this model because the filaments are undergoing reionization during the time in question, presumably by ionizing radiation coming in from the outside. It is not clear theoretically how external ionizing radiation would affect the aggregation properties of the dark matter except through its effect on the gas. Even a collection of the smallest galaxies has filament gas with the full range of sound speed during reionization.

To evaluate such a model, we computed the bulk velocities of the dark matter and gas as a function of transverse distance from the filament axis.

To improve the accuracy of a velocity profile, we refined the determination of the position and orientation of the filament axes. Anticipating that the gas velocities would be minimal along the axis, a principal component analysis was done using just the gas particles having a transverse velocity less than 5.38 km s^{-1}.[4] The orientation of the newly determined axes was close to that of the original ones, and considerably greater directionality was achieved.

Fig. 22 compares the velocity dispersion profiles of the dark matter and the gas of filaments from lingering-gas galaxies whose average sound speed squared is less than or equal to one in our usual units (see Fig. 5). These are the filaments we have found to best match the predictions of the isothermal model we have put forward in this paper. Despite the uncertainties inherent in this computation, it is striking that the gas velocities are reduced near the axis as would be expected from hydrodynamic effects. The dark matter velocities, by contrast, are greater and are roughly constant out to nearly the assumed extent of the filament.

Eisenstein, Loeb & Turner (1997) have derived a relation between the transverse velocity dispersion and the mass per unit length, Υ, of a collisionless cylinder at virial equilibrium.

$$\Upsilon = \frac{v^2}{G} \qquad (5)$$

where v is the average of the square of the transverse velocity and G is the gravitational constant (Eisenstein et al. 1997).[5] The relation is similar to that for a gravitationally bound, isothermal gas cylinder (equation 1) with the bulk velocity substituted for the sound speed.

Our strategy, to better understand the role of the dark matter, is to examine the total virial budget, taking into account both the sound speed of the gas and the bulk velocities of the dark matter and gas. In an hypothesized virial equilibrium, each source of kinetic energy must be balanced by a mass per unit length for the filament. For simplicity, we have taken the mass per unit length of the gravitationally bound, isothermal cylinder as that necessary to balance the sound speed of the gas. For the bulk velocities, we have taken the mass per unit length for the collisionless counterpart described above (equation 5).

---

[4] All velocities are computed relative to a coordinate system moving with the average velocity of the gas particles within 311 comoving kiloparsecs of the centre of the galaxy.

[5] This differs from equation (13) of these authors by a factor of 2. Their equation refers to line-of-sight velocity.
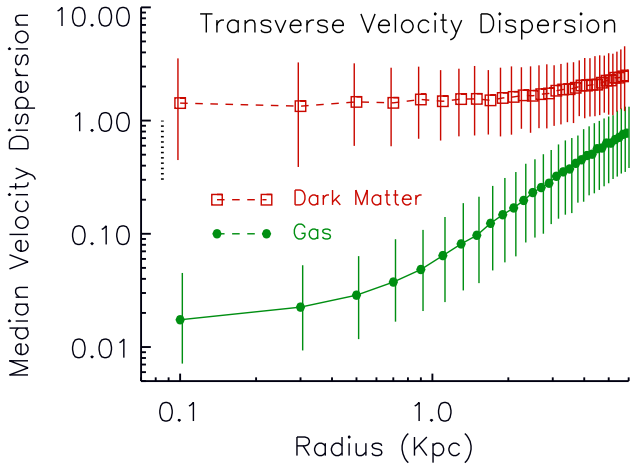
Figure 22. Transverse velocity dispersion profiles. The median transverse velocity dispersion of the dark matter and gas is plotted as a function of distance from the axis of the cylinder. Only filaments from lingering-gas galaxies that have an average sound speed squared of less than one are included. Dark matter is represented by the dashed, red line with squares and gas by a solid, green line with filled circles. The vertical lines at each point on the curves indicate the range of two-thirds of the values. The vertical, dotted, black line at the left shows the range of the sound speed squared of the filaments in our usual units (see Fig. 5). The units for the sound speed squared are chosen to correspond to the expected mass per unit length (see Fig. 5 for a description of these units). The units for the bulk velocities squared of the gas and dark matter are chosen to be twice that for the sound speed in order to account for the difference between equations (1) and (5). The unit corresponds to a velocity of 25.7 km s^{-1}.
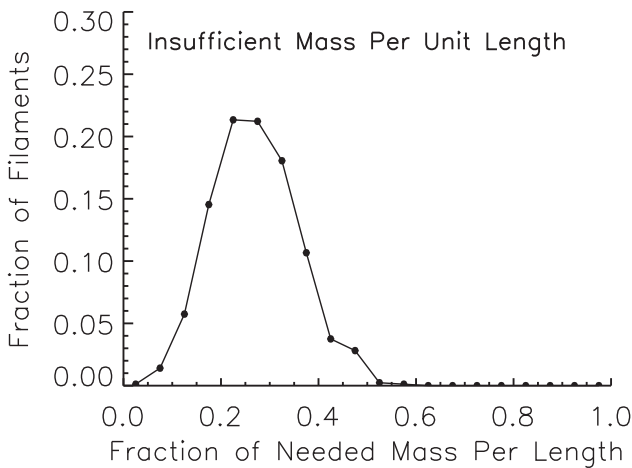

Figure 23. Virial budget. This figure compares the mass per unit length of a filament to that required to balance in a virial equilibrium both the sound speed of the gas and the bulk velocities of the dark matter and gas as explained in Section 4.8.

Fig. 23 shows that the actual mass per unit length is consistently too small for both gas and dark matter to be present together in a virial equilibrium. This figure is a histogram for filaments from lingering-gas galaxies having a sound speed squared less than or equal to one, using our usual units. These are the filaments we have found to match our isothermal cylinder model the best as shown in Fig. 17. The bin on the abscissa is computed by taking the total mass per unit length of the filament and dividing it by the mass per
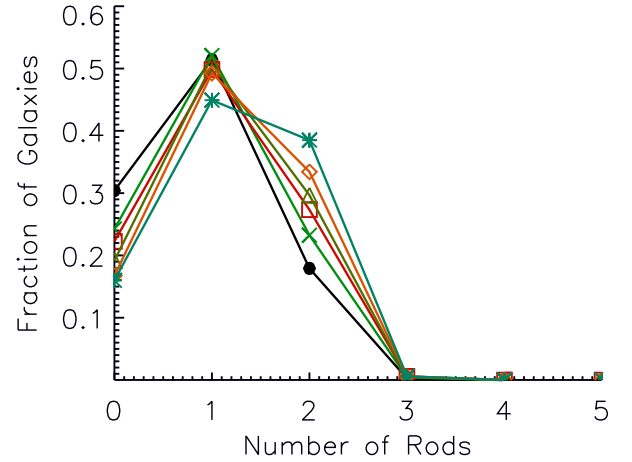

Figure 24. Number of rods per galaxy. Data are shown for each of the six redshifts studied: 8.90 (black, filled circles), 8.09 (green X's), 7.33 (red squares), 6.69 (dull green triangles), 5.85 (orange diamonds), and 5.134 (blue stars).

unit length required to balance both the sound speed of the gas and the bulk velocities of the dark matter and gas.

These results make it hard to justify a model in which the gas is part of a dark matter structure at virial equilibrium. Taking the confines of the filament out to a larger radius may not solve the problem. The periphery typically has an overdensity of only a few compared to a central overdensity in the thousands. Furthermore, the otherwise mostly constant velocity of the dark matter increases at large radius.

We suggest that only the gas of these filaments is close to virial equilibrium. This supposition fits with the fact the lingering-gas galaxies are the ones that are the best match to a gravitationally bound, isothermal gas cylinder. In these galaxies, the dark matter collapses into the forming galaxy more rapidly than does the gas. The moving dark matter provides an environment in which the gravitational constant appearing in the isothermal gas cylinder equations is effectively altered because of the potential energy of the dark matter.

4.9 Number and alignment of filaments

If the filaments in the simulation correspond to the rods of the model, we might expect to see for each galaxy two filaments protruding from the centre of the galaxy that are roughly aligned end-to-end.

Fig. 24 shows that the number of filaments identified for each galaxy is generally no more than two.[6] The six different curves are histograms of the number of filaments for a galaxy at the six redshifts studied. In keeping with the model, in the few cases where more than two were found, only the two most massive were retained for further analysis.

When two segments are present at the same time for a galaxy, the preferred angle between their directions is close to 180°, as if the segments were part of a single, straight rod passing through the centre of collapse. This finding dovetails nicely with the simple paradigm for successive collapse in three dimensions.

---

[6] The filaments used for the graphs in this section are taken from the collection of filaments before they are culled by the range test and the sphere of influence as described in Appendix A.
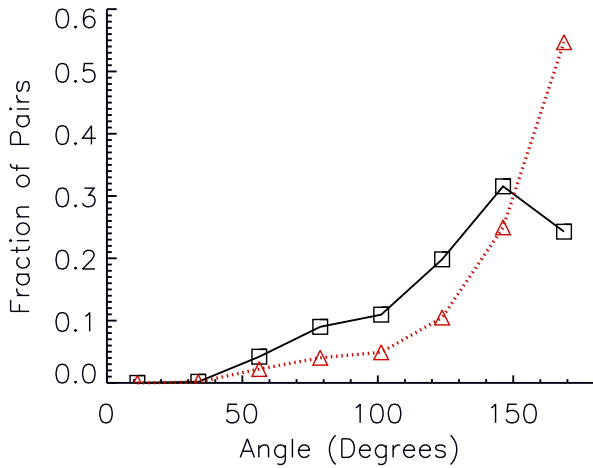
Figure 25. Angle between filament segments. Black, solid line with squares shows a histogram of the angle between the two segment directions in cases where two are found. Red, dotted line with triangles shows the same results when the entries have been weighted by the reciprocal of the sine of the angle.

The black, solid line with squares in Fig. 25 shows a histogram of the angles between the directions of pairs of segments. Results for the six redshifts have been pooled, since the individual results are very similar. The red, dotted line with triangles shows the same histogram with entries weighted by the reciprocal of the sine of the angle. This latter plot is suited to a situation in which the two filaments are assumed to come together in three dimensions rather than forming within a predetermined plane.

In this paper, for clarity, we have called each rod protruding from the centre of the galaxy a filament even though it is attractive theoretically to envision the collapse of a single filament passing through the centre of the galaxy.

5 DISCUSSION

The theme of this paper is that the gas in the intergalactic filaments during the first gigayear can be best understood in terms of simple hydrodynamic principles. In contrast, the dark matter can be understood in terms of the spherically symmetric collapse of an overdensity in an expanding universe.

The filaments undergoing reionization fit the isothermal model best. These filaments tend to have dark matter spread roughly evenly over the entire length. Isothermal cylinders may also be present at later times, but be harder to demonstrate because large dark matter clumps may negate the assumption of uniform mixing.

It is important to emphasize that the filaments we see should be distinguished from the generally larger ones others study at lower redshifts, which often contain within them multiple galaxies. Most papers on the cosmic web have dealt with these massive, later structures.

Eisenstein et al. (1997) have described a method for determining the dynamical mass per unit length of a massive filament containing hundreds of galaxies such as might be observed in redshift surveys at low redshift. The method can be used to estimate the mass-to-light ratios of these filaments. The method is impressive and has theoretical antecedents in common with our model. However, the method is not easily applicable to the very small filaments associated with the galaxies of the first gigayear.

Danovich et al. (2012) have reported that galaxies tend to be at the centre of three filaments contrary to our findings. We also often see more than two filaments extending from a single point. However, we believe that these are likely to be the result of later collisions among filaments. Most of the 1200 largest galaxies can be traced back to an early stage when no more than two roughly end-to-end filaments are present.

To study the numbers and properties of filaments, it is necessary to identify them in an algorithmic fashion free of subjective bias. We find that visual inspection can be deceptive. A plane viewed edge on or the intersection of two planes can appear as a spurious filament. In addition, some of the filament segments are difficult to pick out from the background by eye.

We believe that our criteria for selection of filament candidates are good, and that it is not unreasonable to discard additional faint filaments that may be seen by eye.

It should also be appreciated that, at early times, the centre of a future galaxy connecting two end-to-end filaments may not be apparent upon casual inspection. Rather it may appear to the eye simply as a point on a single continuous filament. This situation could lead to an apparent preference for more than two filaments emanating from a single galaxy.

We argue that, during the reionization process, the gas assumes a structure that can be understood in terms of a gravitationally bound, isothermal cylinder at equilibrium at about 10^4 K. We find that this temperature, close to the Lyman alpha cooling floor, is tightly maintained during reionization. This temperature regulation may be important in the stability of the cylinders during this period.

The change in sound speed during reionization can be seen reflected in a change in the mass per unit length of the cylinder (Fig. 5). We consider this finding together with the proportionality constant to be strong evidence for gravitationally bound, isothermal cylinders.

To further justify our emphasis on the importance of the gas component, we explored the virial consequences of a more conventional model in which the structure is primarily determined by the aggregation properties of dark matter. There appeared to be too little mass per unit length for such a model.

It is important to note that the simulation follows in detail the ionization of the gas by radiation from the actual sites of stellar formation. This is in contrast to many simulations that merely impose a uniform radiation field and thus might miss such structural nuances. For such simulations, we would not expect dramatic changes in the physics of the gas in the filaments because there is very little stellar material in the filaments. However, the time course of reionization would probably be altered with the result that there would be fewer filaments with intermediate ionization stages. Demonstration of isothermal cylinders might then be more difficult as a result.

We find remarkable uniformity in the behaviour of the dark matter of the 1200 largest galaxies in the simulation. These galaxies range in total mass, including dark matter, gas, and stars, over two orders of magnitude. The dark matter collapse follows closely the spherically symmetric cycloid model at least through turnaround. The overdensity at turnaround agrees roughly with theoretical expectation. The matter collapses initially into a rough plane and then into a one-dimensional structure within the plane, resulting in up to two filaments protruding from the centre of the galaxy oriented end to end. At any time, approximately three quarters of the galaxies have at least one filament emerging from it.

An outstanding problem in cosmology is the discrepancy between the observed number of satellite galaxies of the Milky Way and the predicted number from simulations using dark matter only (Kauffmann et al. 1993). Our results suggest a mechanism that suppresses the entry of gas into dark matter haloes. This phenomenon would be in contrast to the expulsion of gas from haloes by heating and photoionization.

One might imagine that filaments would facilitate the entry of gas into the halo by restricting its angular momentum. However, our results argue that, on balance, the gas that can be accommodated into an isothermal cylinder is retarded in its motion.

A simulation with greater resolution would be desirable to confirm and expand upon these results. Higher resolution might reveal structures important in the formation of galaxies smaller than the ones studied here. It would be interesting to see if there is a minimum galaxy size that can form according to our filament model. Would very small galaxies form very early when the temperature is substantially lower than the Lyman alpha cooling floor?

A higher resolution would also help to establish whether the dark matter really is as clumpy compared to the gas as it appears. Sometimes increasing resolution can expose artefacts arising from the discreteness of the simulation elements. We would not expect a higher resolution to reveal the gas in the filaments as fragments rather than continuous. This is because, when discreteness is important, it is usually the lower resolution simulation that is fragmented rather than the higher one. For a discussion of discreteness effects, see Power et al. (2016).

Reionization is regarded as a watershed event in the history of the universe. A galaxy that formed before reionization could retain an ancient population of stars that could not have formed afterward if the galaxy were too small. Brown et al. (2014) have argued from an analysis of individual stars that some ultrafaint dwarf satellites of the Milky Way are indeed such galaxies that have survived to the present day. The galaxies in our study all began their formation prior to reionization. We do not know their likely fate, but it is plausible that they could share common features with some small galaxies observed at redshift zero. It is thus not unreasonable to compare our galaxies with galaxy populations observed today that exhibit the 'too big to fail' effect.

A comprehensive consideration of the 'too big to fail' phenomenon is beyond the scope of this paper. We note, however, that our model differs from most of the other ones in focusing on the transport of gas into the galaxy, rather than on baryonic effects and star formation within the galaxy (see for example Governato et al. 2012; Zolotov et al. 2012; Brooks et al. 2013; Vera-Ciro et al. 2013; Arraki et al. 2014; Brooks & Zolotov 2014; Madau, Weisz & Conroy 2014; Jiang & van den Bosch 2015; Pawlowski et al. 2015; Agertz & Kravtsov 2016; Read, Agertz & Collins 2016; Wetzel et al. 2016; Zhu et al. 2016).

A detailed analysis of the motion of gas into galaxies is beyond the scope of this paper. Our model is consistent with the 'cold mode' of galaxy accretion. We see no evidence for a hot gas stage in the formation of our galaxies. We have argued from rates of collapse of the dark matter and gas that the gas moves into the galaxy along a single, linear filament.

An important open question involves the timing and mechanism of the reionization of the universe. To evaluate the role of ionizing radiation from stars one must know the fraction of stellar radiation that escapes from its point of origin. It is clear that the gas surrounding the centre of collapse of a galaxy is not spherically symmetric. Our results may provide a more realistic starting point for such calculations.

Finally, our model suggests the central presence of gas at a very early time in the formation of the galaxy halo. Perhaps this gas contributes to the formation of a 'cored' halo profile as opposed to the 'cuspy' one suggested from simulations containing only dark matter (Gilmore et al. 2007; Evans, An & Walker 2009; de Blok 2010; Strigari, Frenk & White 2010; Amorisco & Evans 2012; Martinez 2015).

6 SUMMARY

We propose a model for the development of intergalactic filaments during the first gigayear of the universe. In this model, the mass per unit length and structure of the filament is determined, not by the potential well of the enclosing dark matter, but by the hydrodynamic properties of the gas.

The model is described in the context of galaxy formation. Up to two extended filaments may protrude from the centre of the collapsing galaxy. They tend to be oriented end-to-end as if they comprised a single structure. The total mass per unit length of a filament segment is proportional to the square of the sound speed of the gas with a proportionality constant equal to that predicted for a gravitationally bound, isothermal cylinder. The sound speed of a gas filament depends only upon its temperature and ionization state and not upon the density. These structures generally contain gas and dark matter in roughly the cosmic ratio. The dark matter contributes to the gravitational field in proportion to its abundance as if it were uniformly mixed with the gas.

The dark matter of each galaxy collapses according to the simplest model for a spherically symmetric overdensity in an expanding universe. This cycloid profile is followed until sometime after turnaround. The overdensity of the material at turnaround agrees with theoretical predictions.

After reionization, the average gas fraction of a filament segment may increase as the collapse of dark matter progresses.

Overall the dark matter collapses to roughly the same extent for each galaxy. However, the gas collapse varies. Three types of galaxies are distinguished. In the 'plunging-gas' galaxies, the gas collapses as fast or faster than the dark matter. These galaxies appear to collapse from overdensities having far too much matter to form a gravitationally bound, isothermal filament under the ambient thermal conditions. In the 'retreating-gas' galaxies, the gas fails to move towards the halo and may expand with the universe. These galaxies appear to collapse from overdensities having too little matter. Finally, in the 'lingering-gas' galaxies, the gas collapses but more slowly than does the dark matter. These appear to have available masses in a suitable range to form gravitationally bound, isothermal cylinders. Presumably, the gas that can be accommodated in the isothermal structure is retarded in its motion, whereas excess gas can proceed unhindered.

For the lingering-gas galaxies, the different overall rates of migration of the dark matter and gas predict the final baryon fraction of the galaxy under a simple assumption of uniform, filamentary accretion, but are inconsistent with spherical accretion.

The model works for a galaxy mass range that includes that of the so-called too big to fail galaxies and may explain the peculiar absence of these galaxies from observational surveys.

The model may provide a mathematical framework for understanding a variety of open questions about structure formation in the early universe. The sizes of the structures in this model suggest a minimum simulation resolution that may be necessary to recreate the effects seen here. In addition, the model may contribute to

our intuition about the roles of dark matter and gas in structure formation.

ACKNOWLEDGEMENTS

REFERENCES

Agertz O., Kravtsov A. V., 2016, ApJ, 824, 79
Amorisco N. C., Evans N. W., 2012, MNRAS, 419, 184
Arraki K. S., Klypin A., More S., Trujillo-Gomez S., 2014, MNRAS, 438, 1466
Bertschinger E., Gelb J. M., 1991, Comput. Phys., 5, 164
Binney J., 2004, MNRAS, 347, 1093
Birnboim Y., Dekel A., 2003, MNRAS, 345, 349
Boylan-Kolchin M., Springel V., White S. D. M., Jenkins A., Lemson G., 2009, MNRAS, 398, 1150
Boylan-Kolchin M., Bullock J. S., Kaplinghat M., 2011, MNRAS, 415, L40
Boylan-Kolchin M., Bullock J. S., Kaplinghat M., 2012, MNRAS, 422, 1203
Brooks A. M., Zolotov A., 2014, ApJ, 786, 87
Brooks A. M., Governato F., Quinn T., Brook C. B., Wadsley J., 2009, ApJ, 694, 396
Brooks A. M., Kuhlen M., Zolotov A., Hooper D., 2013, ApJ, 765, 22
Brown T. M. et al., 2014, ApJ, 796, 91
Cen R., Ostriker J. P., 1993, ApJ, 417, 415
Conselice C. J., 2014, ARA&A, 52, 291
Danovich M., Dekel A., Hahn O., Teyssier R., 2012, MNRAS, 422, 1732
de Blok W. J. G., 2010, Adv. Astron., 2010, 789293
Dekel A., Birnboim Y., 2006, MNRAS, 368, 2
Dekel A. et al., 2009, Nature, 457, 451
Eisenstein D. J., Loeb A., Turner E. L., 1997, ApJ, 475, 421
Evans N. W., An J., Walker M. G., 2009, MNRAS, 393, L50
Ferrero I., Abadi M. G., Navarro J. F., Sales L. V., Gurovich S., 2012, MNRAS, 425, 2817
Frenk C. S., White S. D. M., 2012, Ann. Phys., 524, 507
Frieman J. A., Turner M. S., Huterer D., 2008, ARA&A, 46, 385
Garrison-Kimmel S., Boylan-Kolchin M., Bullock J. S., Kirby E. N., 2014, MNRAS, 444, 222
Gilmore G., Wilkinson M. I., Wyse R. F. G., Kleyna J. T., Koch A., Evans N. W., Grebel E. K., 2007, ApJ, 663, 948
Gnedin N. Y., 1995, ApJS, 97, 231
Gnedin N. Y., Bertschinger E., 1996, ApJ, 470, 115
Governato F. et al., 2012, MNRAS, 422, 1231
Harford A. G., Hamilton A. J. S., 2011, MNRAS, 416, 2678
Harford A. G., Hamilton A. J. S., Gnedin N. Y., 2008, MNRAS, 389, 880
Jiang F., van den Bosch F. C., 2015, MNRAS, 453, 3575
Katz N., Keres D., Dave R., Weinberg D. H., 2003, in Rosenberg J. L., Putman M. E., eds, Astrophysics and Space Science Library, Vol. 281, The IGM/Galaxy Connection. The Distribution of Baryons at z=0, How Do Galaxies Get Their Gas. Kluwer Academic Publishers, Dordrecht, p. 185
Kauffmann G., White S. D. M., Guiderdoni B., 1993, MNRAS, 264, 201
Kereš D., Katz N., Weinberg D. H., Davé R., 2005, MNRAS, 363, 2
Kereš D., Katz N., Fardal M., Davé R., Weinberg D. H., 2009, MNRAS, 395, 160
Klypin A., Kravtsov A. V., Valenzuela O., Prada F., 1999, ApJ, 522, 82
Klypin A., Karachentsev I., Makarov D., Nasonova O., 2015, MNRAS, 454, 1798
Kravtsov A. V., Borgani S., 2012, ARA&A, 50, 353
Madau P., Weisz D. R., Conroy C., 2014, ApJ, 790, L17
Martinez G. D., 2015, MNRAS, 451, 2524
Moore B., Ghigna S., Governato F., Lake G., Quinn T., Stadel J., Tozzi P., 1999, ApJ, 524, L19
Ocvirk P., Pichon C., Teyssier R., 2008, MNRAS, 390, 1326
Ostriker J., 1964, ApJ, 140, 1056

Papastergis E., Shankar F., 2016, A&A, 591, A58
Papastergis E., Giovanelli R., Haynes M. P., Shankar F., 2015, A&A, 574, A113
Park C., 1990, MNRAS, 242, 59
Pawlowski M. S., Famaey B., Merritt D., Kroupa P., 2015, ApJ, 815, 19
Peacock J. A., 1999, Cosmological Physics. Cambridge Univ. Press, Cambridge, p. 488
Power C., Robotham A. S. G., Obreschkow D., Hobbs A., Lewis G. F., 2016, MNRAS, 462, 474
Read J. I., Agertz O., Collins M. L. M., 2016, MNRAS, 459, 2573
Rees M. J., Ostriker J. P., 1977, MNRAS, 179, 541
Somerville R. S., Davé R., 2015, ARA&A, 53, 51
Stodólkiewicz J. S., 1963, Acta Astron., 13, 30
Strigari L. E., Frenk C. S., White S. D. M., 2010, MNRAS, 408, 2364
Sugerman B., Summers F. J., Kamionkowski M., 2000, MNRAS, 311, 762
Tollerud E. J., Boylan-Kolchin M., Bullock J. S., 2014, MNRAS, 440, 3511
Vera-Ciro C. A., Helmi A., Starkenburg E., Breddels M. A., 2013, MNRAS, 428, 1696
Wetzel A. R., Hopkins P. F., Kim J.-h., Faucher-Giguère C.-A., Kereš D., Quataert E., 2016, ApJ, 827, L23
White S. D. M., Rees M. J., 1978, MNRAS, 183, 341
Zel'dovich Y. B., 1970, A&A, 5, 84
Zhu Q., Marinacci F., Maji M., Li Y., Springel V., Hernquist L., 2016, MNRAS, 458, 1559
Zolotov A. et al., 2012, ApJ, 761, 71

APPENDIX A: ALGORITHM FOR FILAMENT IDENTIFICATION

Each filament is selected in the context of a forming galaxy. Fig. A1 shows the geometry for this selection for an example galaxy. The selection takes place in a comoving coordinate system whose centre is the centre of mass of the collapsing dark matter particles of the galaxy. Unlike the gas particles, the individual dark matter particles of a galaxy can be followed throughout the simulation. The *XY*-plane is set to the plane of the gas as determined by a principal component analysis of the gas particles within a sphere of radius 266 kpc. The large black rectangle in the Fig. A1 shows this *XY*-plane. Annuli above (red) and below (green) the plane determine a volume that is divided into equal bins by the light blue rectangles.
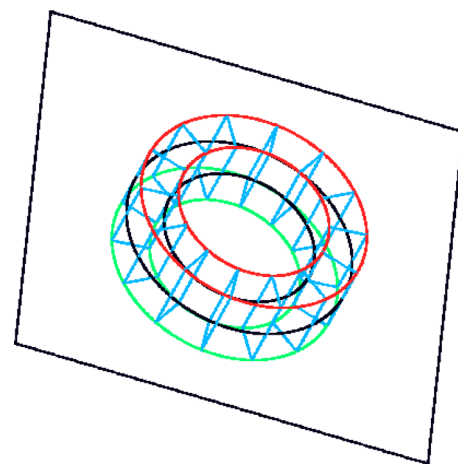

Figure A1. Coordinate system for identification of intergalactic filaments. Outlined in black is the *XY*-plane with the origin of the coordinate system at its centre. One pair of annuli is shown with members above (red) and below (green) the central plane, The volume between the two annuli is divided into equal, azimuthal bins. The intersection of the volume with the plane is shown in black. Planes marking the boundaries of the bins are outlined in light blue.
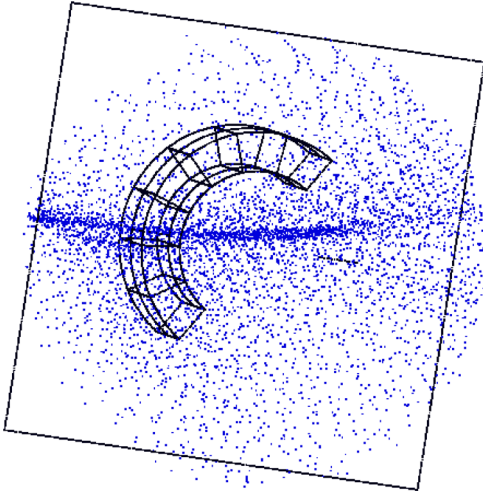
Figure A2. Identification of a filament extending from the centre of a galaxy. The centre of the collapsing dark matter is at the centre of the coordinate system shown in Fig. A1, and the plane shown in that figure is oriented to the plane of the gas. The gas particles in a region surrounding the centre of a collapsing galaxy are shown in blue. For clarity, only some of the bins are shown.

The intersection of the bins with the plane are shown by the black annulus. The annulus is defined by two radii of 88.8 and 133.2 kpc.

A bin having more than twice the average amount of gas per bin is considered to contain a filament. In cases where neighbouring bins of the annulus both meet this criterion, the gas in both bins is merged and analysed together. The filament identification process is completely defined by this algorithm. There are no subjective elements.

The algorithm identifies visually clear segments that are usually part of longer filaments extending radially from the centre of collapse of the galaxy. Also identified, and therefore included in our analysis, are structures that may not be readily identified or interpreted by eye.

These filament segments are used in Section 4.9 to compare the relative orientations of the filaments with the prediction of the model. However, for the analyses in the remaining sections, the set of segments is further culled using a 'range test'. In this test, the filament segment is divided into three parts. To pass the test, the mass of gas in each part can differ from the average of the three parts by no more than 20 per cent. This test ensures that the identified structure grossly resembles a filament. This is important because we do not allow any subjective inspection of a segment to influence whether it is included.

In addition, we require that the sphere of influence of the galaxy cover at least half of the filament segment in question. This is done to ensure that nearby galaxies do not result in the selection of the same filament. The sphere of influence is considered to be a sphere with radius equal to the turnaround radius in comoving coordinates centred at the centre of the galaxy at the time in question.

A total of 2300 filament segments selected from the six redshifts considered survived all tests.

For structural analysis, the orientation of each segment is determined more precisely using a principal component analysis.

This paper has been typeset from a TeX/LaTeX file prepared by the author.